10th International Conference on Composite Science and Technology
ICCST/10
A.L. Araújo, J.R. Correia, C.M. Mota Soares, et al. (Editors)

CHARACTERISATION OF MELT PROCESSED NANOCOMPOSITES OF POLYAMIDE 6 SUBJECTED TO UNIAXIAL-DRAWING

B. Mayoral[1]*, E. Harkin-Jones[2], P. Noorunnisa Khanam[3], M.A. AlMaadeed[3,4], M. Ouederni[5], Mark Tweedie[2], D. Sun[1*] and A. Hamilton[1]

[1]School of Mechanical and Aerospace Engineering, Queen's University Belfast,
Belfast BT9 5AH, United Kingdom
b.mayoral@qub.ac.uk, d.sun@qub.ac.uk, a.hamilton@qub.ac.uk

[2]School of Engineering, University of Ulster,
Newtownabbey, Antrim BT37 0QB, United Kingdom
e.harkin-jones@ulster.ac.uk, m.tweedie@ulster.ac.uk

[3]Center for Advanced Materials, [4]Materials Science and Technology Program,
Qatar University, 2713 Doha, Qatar
noor.pathan@qu.edu.qa, m.alali@qu.edu.qa

[5] Research & Development, Qatar Petrochemical Company (QAPCO), Doha, Qatar
MOuederni@qapco.com.qa

Keywords: Nanocomposites, Graphene nanoplatelets, Polymer, Melt processing, Extrusion.

Summary: *In this paper, the processing and characterization of Polyamide 6 (PA6) nanocomposites containing graphite nanoplatelets (GNPs) is reported. PA6 nanocomposites were prepared by melt-mixing using an industrial, co-rotating, intermeshing, twin-screw extruder. A bespoke screw configuration was used that was designed in-house to enhance nanoparticle dispersion into a polymer matrix. The effects of nanofiller content and uniaxial stretching on the bulk properties of the PA6/GNPs nanocomposites were investigated. The crystalline structures of PA6/GNPs nanocomposites are related to thermal treatment, stress history and the presence of moisture and nanofillers. DSC, Raman and XRD studies show an increase in crystallinity with increasing GNPs content as a result of the heterophase nucleation effect. The effect of uniaxial stretching on PA6 nanocomposites was investigated by drawing specimens heated at temperatures below the melting temperature. DSC and Raman studies of the drawn samples show an increase in crystallinity as the GNP content increases due to the strain induced crystallization. Analysis of the rheological data indicates that a percolation threshold was reached at GNPs contents of between 10–15wt%. An increase in tensile modulus of as much as 378% was observed for PA6/M-5* xGnP® *composites, at a filler content of 20wt%. The enhancement of Young's modulus can be attributed to the reinforcing effect of GNPs and their uniform dispersion in the PA6 matrix. The electrical conductivity of the composite also increased with increasing GNPs content, with an addition of 15wt% GNP resulting in a 6 order-of-magnitude increase in conductivity. The electrical percolation threshold for PA6/M-5 composites was reached between 10-15 wt% GNPs. The uniaxial stretching slightly reduces the electrical conductivity in PA6/M5 composites, however, a recovery of the conductive network occurred when the samples were annealed.*

1 INTRODUCTION

In recent years graphene, due to its outstanding properties, has become the topic of much research activity [1-4]. Single layer graphene with a Young's modulus of 1TPa and an ultimate strength of 130 GPa is the strongest material ever measured [4]. As a conductor of electricity it performs as well as copper. As a conductor of heat it outperforms all other known materials. It is almost completely transparent, yet so dense that not even helium, the smallest gas atom, can pass through it [5]. Graphene which is a 2D monolayer of carbon atoms has a significant number of potential advantages over its 1D cousin, carbon nanotubes. Because it is 2D, property enhancement will also be 2D [6]. An even greater advantage is likely to emerge in the future as the use of CNTs in plastic components is provoking fears about toxicity potential [7] that, due to its 2D nature, graphene is unlikely to exhibit. In comparison with nanoclays, graphene has the huge advantage of being conductive coupled with superior mechanical properties (178 GPa modulus compared with 1TPa for Graphene). There is also the potential of much larger particle dimensions than available with naturally occurring nanoclays. The potential applications for this material are enormous particularly if it can be successfully incorporated into polymers by conventional polymer processing routes.

Applications include low cost, light weight, EMI shielded computer housings and cables, anti-static packaging, lightweight, high strength automotive and aerospace components, high barrier packaging and smart clothing/personal sensor systems. The multifunctionality of graphene combined with its relatively low cost methods of production makes this a unique material.

Many researchers globally are currently engaged in finding the best way of producing high quality graphene on a large scale. Recent research by Drzal et al. has shown that it is feasible to exfoliate natural graphite into nanoplatelets having thicknesses <10nm and diameters of tens of microns in size [8, 9]. This material, which is known as exfoliated graphite nanoplatelets (xGnP®), has a platelet morphology with a surface area of more than $100m^2/g$, a thickness of ≤10nm and a diameter that can be controlled by adjusting the milling conditions. Since xGnP is based on very affordable and still abundant natural graphite, the cost is expected to be substantially lower than other carbon materials [10].

The objective of this research was to assess the effect of GNPs on the mechanical and electrical properties of thermoplastic polymers processed via melt mixing. Polyamide 6 (PA6) was chosen as the matrix material due to its engineering property profile and significant commercial interest. The morphology, rheological, thermal, structural, mechanical and electrical behaviour of the composites were investigated to assess the influence of GNP content and extruder screw speed on the properties of the resulting nanocomposites.

2 EXPERIMENTAL

2.1 Materials

BASF Ultramid B40L (Relative Viscosity 3.89 - 4.17) Polyamide 6 (PA6) was supplied in pellet form by Ultrapolymers. The PA6 pellets were cryogenically ground to a fine powder of micro-scale particles using a Wedco SE-12 UR pilot plant grinding mill at 7000 rpm and a gap size set to 400 µm using liquid nitrogen for temperature regulation. xGnP® Graphene Nanoplatelets were supplied by XG Sciences. Technical specifications of these GNPs are detailed in Table 1:

GRADE	# layers	Thick. (nm)	Diam. (µm)	Surf. Area (m^2/g)
M-5	18-24	6-8	5	120-150

Table 1: xGnP® Graphene Nanoplatelet technical specifications.

2.2 Composite Preparation

The ground PA6 powder was dried at 80^{0}C for 12 hours prior to mixing. Pre-dried PA6 powder and GNPs, were pre-mixed at 1 wt%, 3wt%, 5 wt%, 7.5 wt% and 10 wt% graphene using a Thermo Scientific Prism Pilot 3 High Speed Mixer at 2000rpm for 2 mins. The melt-mixing process was performed using a co-rotating intermeshing twin-screw extruder (Collin GmbH), having a screw diameter of 25 mm and a barrel length of 750 mm (L/D=30). On exiting the capillary die the extrudate was drawn through a cooled water bath at a constant haul off rate and pressure. The extrudate was dried by passing through an air ring and then pelletized using a Collin Pelletiser. A bespoke screw configuration designed to enhance nanoparticle dispersion into polymeric matrices was used [11]. The process conditions used for extrusion are shown in Table 2. The extruded pellets were dried in the oven at 80°C for 4 hours before compression moulding. Samples were compression moulded in a platen press at 250°C for 3 mins at 150 bars.

Extruder Zones	Z1	Z2	Z3	Z4	Z5	Z6	Die
Temperature (°C)	185	245	240	240	240	235	240
Screw Rotation direction		Co-rotating					
Screw Speed (rpm)		High Speed=200rpm					
GNPs Loading (wt%)	1%	3%	5%	7.5%	10%	15%	20%

Table 2- Process conditions set up for PA6/GNP extrusion in the twin screw extruder.

2.3 Secondary Processing: Uniaxial Drawing (stretching)

Uniaxial drawing was carried out using an Instron 5564 Universal Tensile Tester fitted with an environmental chamber to enable uniaxial drawing of the samples at elevated temperatures. Type IBA samples from ISO 527-2 were die cut from compression moulded plaques. Samples were drawn at a speed of 50 mm/min to a maximum nominal strain of 60% at temperatures ranging from 120°C to 220°C in order to optimise stretching. The most successful stretching temperatures were found to be 180°C for unfilled PA6, PA6/5%M-5 and PA6/10%M-5 and 200°C for PA6/15%M-5 and PA6/20%M-5. Uniaxial stretching was not always homogeneous and necking occurred in some samples due to the reduced width.

2.4 Characterization

GNP dispersion was investigated using oscillatory melt rheology. Dynamic rheological measurements were performed using an AR-G2 Oscillatory Rheometer and Rheology Advantage Instrument Control AR Software. The measurements were carried out in oscillatory shear mode using parallel plate geometry (Standard ETC Steel plate, 25 mm diameter, 1 mm gap) at 240 °C. Frequency sweeps from 100 rad/s to 0.1 rad/s were carried out at low strains (1%) which were shown to be within the linear viscoelastic limit of all the materials of interest.

Wide-angle X-ray diffraction (WAXRD) of compression moulded samples of PA6 and PA6/xGnP composites were recorded using a PANalytical X'Pert PRO diffractometer with Cu-K_α radiation (λ=1.5406 Å) at a scanning rate of 0.0.2°/min over the range 2–60°(2θ).

Raman spectroscopy was conducted using a LabRam300 instrument, with a 10 mW HeNe laser (wavelength 632.81 nm) and a 50X focusing objective. A neutral density filter at 50% reduced the intensity of the laser at full power and avoided sample damage. A confocal hole of 400 μm, a spectrometer slit width of 200 μm, and a diffraction grating of 1800 grooves/mm were used to acquire measurements. The instrument was calibrated against an unoxidised Si sample, to adjust the peak to 520.7 cm^{-1}. A spectral range from 100 cm^{-1} to 3500 cm^{-1} was measured. A sample integration time of 60 s per window was used. The CCD was multi-stage Peltier-cooled to an operational temperature of -70°C.

Differential scanning calorimetry (DSC) was performed on samples of unfilled PA6 and PA6/GNP composites using a Perkin–Elmer DSC model 6 under an inert nitrogen atmosphere using a heating and cooling rate of 10 K/min. between 30°C and 275°C. In all cases the samples were held at 275 °C for 3 min., then cooled to 30°C at 10K/min. and reheated to 275°C at 10 K/min. to ensure complete melting of the crystalline fraction of PA6 and to remove thermal history. The apparent crystalline content of the composites was determined using a value of 191J/g for the heat of fusion for a theoretically 100% crystalline PA6.

Tensile tests were carried out following BS EN ISO 527-1: 1996 and using an Instron 5564 Universal Tester with a clip-on extensometer at room temperature and a 2 kN load cell. Samples were prepared by compression moulding, from which dumbbell-shaped samples (type 1BA) were cut using a stamping press. For elastic modulus measurements, nominal strain was determined using an extensometer attached on the narrow portion of the dumb-bell samples at a crosshead speed of 1 mm/min and a gauge length of 25 mm. Elastic modulus was determined from the slope of the regression of the stress-strain data between 0.05 - 0.25 % strain.

Volume resistivity measurements were performed on compression moulded samples of 1 mm thickness for all nanocomposites. For high resistivity samples, a Keithley electrometer (Model 6517A) equipped with an 8009 test fixture with circular samples of diameter 60 mm was used. The sample of interest was placed between two circular electrodes and the volume resistivity measured by applying a DC voltage potential across opposite sides of the sample and measuring the resultant current through the sample. This test conforms to ASTM D-257. For more conductive samples (< 10^7 Ω cm) strips with dimensions of 50×10 mm^2 were cut from the sheets and measured using a Keithley electrometer (Model DMM 2000) using a two-point test fixture (contact wires with 50 mm between the measuring electrodes).

3 RESULTS AND DISCUSSION

The results of the oscillatory melt rheology study, including complex viscosity (η*) and inverse loss tangent (tan δ)$^{-1}$, are shown in the form of log-log plots in Fig.1 for unfilled PA6 and PA6/GNPs composites.

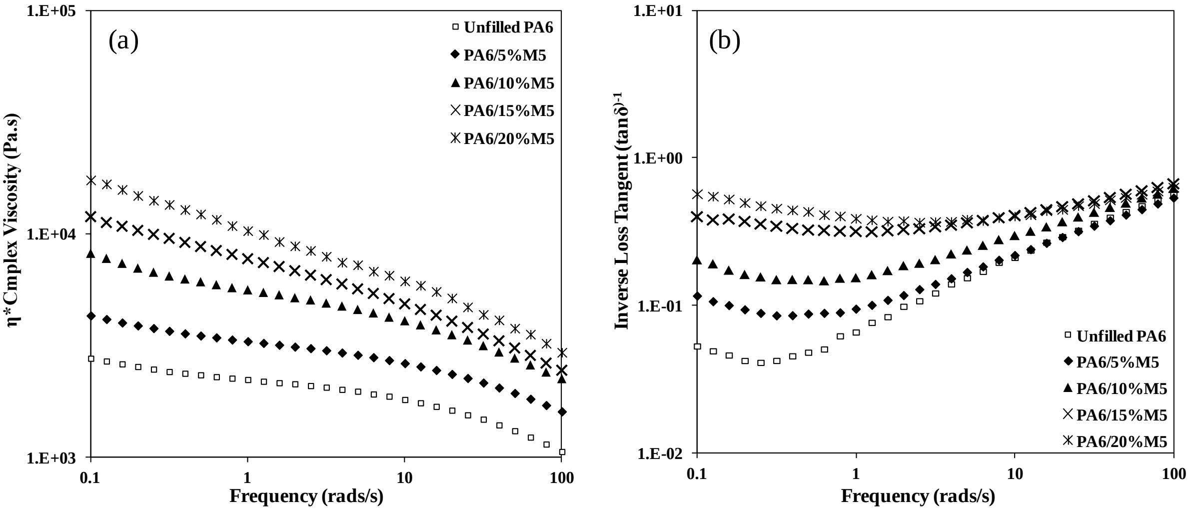

Fig.1: Variation in (a) complex viscosity (*η**) and (b) inverse loss tangent (tan δ)$^{-1}$ as functions of frequency at 240°C for unfilled PA6 and PA6/M5 composites.

Unfilled PA6 exhibits non-Newtonian behaviour, where viscous behaviour dominates at low frequencies (G'~ω^2) and polymer chain entanglements at higher frequencies, while the composites with 5 wt%, 10 wt%, 15 wt% and 20 wt% GNPs exhibit a clear transition to shear-thinning behaviour. As expected, the addition of high aspect ratio and high modulus GNPs increases η* of the PA6 matrix by an order of magnitude (Fig. 1(a)). Similar trends have been reported in other polymer nanocomposites systems [11-14]. A rheological percolation threshold was obtained between 10-15 wt% GNPs, as indicated by an increase in *η** at low frequencies where the rheological response of the composite is more like a 'pseudo-solid' than a molten liquid. From a plot of inverse loss tangent (tan δ^{-1}) versus frequency (Figure 1(b)) it is possible to observe further evidence for the formation of a percolated network [15]. At low frequencies, the curves for the 5 wt%, 10 wt%, 15 wt% and 20 wt% GNP composites form a plateau, implying percolation was achieved, as an increase in tan δ^{-1} is a measure of the increase in 'solidity' of the composite. Similar trends were found for PP/MWCNT composites produced by melt-mixing with a rheological percolation ~0.5 wt% MWCNTs being reported [16].

The Young's modulus of neat PA6 and M-5 GNP composites are shown in Table 3. For the PA6/M-5 composites, the tensile modulus shows an increase with respect to the PA6 unfilled of 34% at 5%GNPs, 183% at 10% GNPs and 310% at 15%GNPs addition with a maximum of 6142MPa (378% increase respect PA6 unfilled) at 20 wt% loading.

	Modulus (MPa)	Impr*(%)
PA 6 unfilled	1285.7	
PA6/5%M-5	1726.0	34.3
PA6/10%M-5	3644.8	183.5
PA6/15%M-5	5269.3	309.9
PA6/20%M-5	6142.0	377.7

Table 3: Effect of addition of M-5 GNPs to Young Modulus of PA6 unfilled.

Thermal analysis using DSC was performed to study the effect of GNP addition on the melting and crystallisation behaviour of PA6. The crystallization temperature (T_c), melting temperature (T_m), enthalpies of fusion (ΔH) and crystalline content(X_c) are shown in Table 4.

200rpm	First heat				Cooling		Second heat			
	Tm (^{o}C)	ΔH (J/g)	X_c (%)	Impr (%)	Tc (^{o}C)	ΔH (J/g)	Tm (^{o}C)	ΔH (J/g)	X_c (%)	Impr (%)
PA6 Unfilled	222.6	71.5	37.4		179.6	70.7	222.3	68.0	35.6	
PA6/ 5wt% M-5	222.6	134.5	70.4	88.1	184.5	90.4	222.4	115.3	60.3	69.5
PA6/ 10wt% M-5	222.6	149.4	78.2	108.9	185.2	118.3	222.1	142.0	74.4	108.8
PA6/ 15wt%M-5	224.0	156.4	81.9	118.7	186.4	117.4	223.3	148.7	77.9	118.7
PA6/ 20wt% M-5	224.7	158.9	83.2	122.2	187.7	118.5	223.9	149.4	78.2	119.7

Table 4: Effect of GNPs addition on the thermal properties of unfilled PA6.

The addition of GNPs had little effect on the melting temperature (T_m) of PA6. However, the addition of GNPs significantly increases the crystallinity of the PA6 and Tc is also significantly increased. This is indicative of a strong nucleation effect by the GNPs. Similar trends have been observed in other studies of PA6/GNPs tensile properties, with a maximum Young's Modulus of 2300MPa at 10%GNPs (42% enhancement) [17] and 5.9GPa at 15wt% GNP (168% improvement)[18].

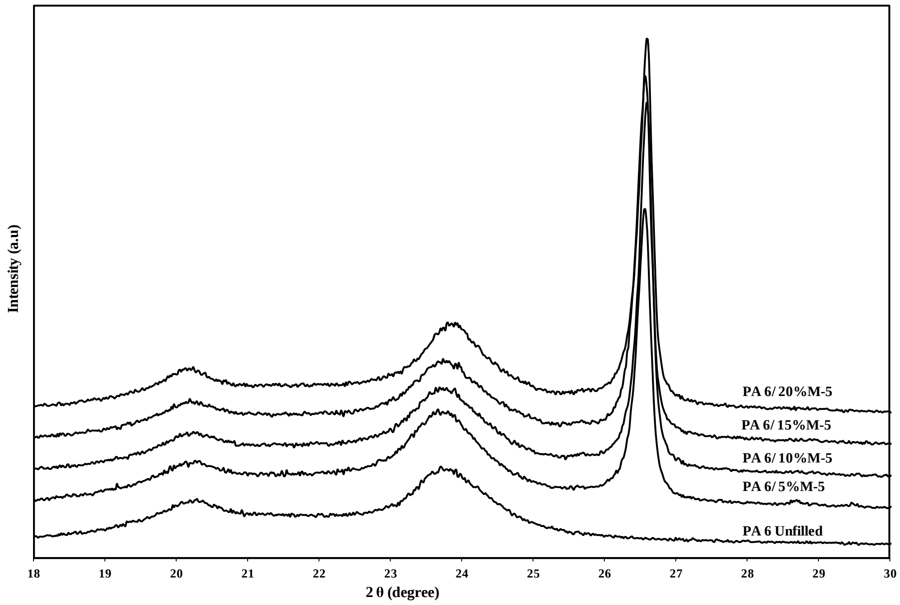

Fig.2: XRD traces for unfilled PA6 and PA6/M-5 composites.

From the XRD results in Fig 2, PA6 exhibits two main diffraction peaks at scattering angles of 2ϴ=20° and 23.7°, attributed to the α100 and α002/202 crystal planes, respectively. There is no clear evidence of a reflection at 2ϴ = 21.4° which is associated with the γ001 crystal planes of PA6. A sharp peak around 26.5° appears for the %GNPs composites which is assigned to the graphite d002 diffraction peak [19]. As %GNPs increases the α100 peak shifts to the left and the α002/202 peak shifts to the right changing slightly their intensity, indicating a change in the preferential growth of the PA6 crystal planes. Similar trends have been reported by Liu et al. in PA6/silicate clays systems [19].

Uniaxial drawing (stretching) of heated PA6 and PA6/GNPs composite samples was carried out and the properties of stretched samples characterised. As expected, increasing the %GNPs increased the yield stress of the material, as shown in Fig.3. The increase in yield stress in the composites is equivalent to the force required to deform the material and may be caused by the greater restriction on molecular mobility or increased entanglement of molecules due to the presence of GNPs [20]. PA6/15%M-5 and PA6/20%M-5 fractured before samples could be stretched to the maximum nominal strain of 60%.

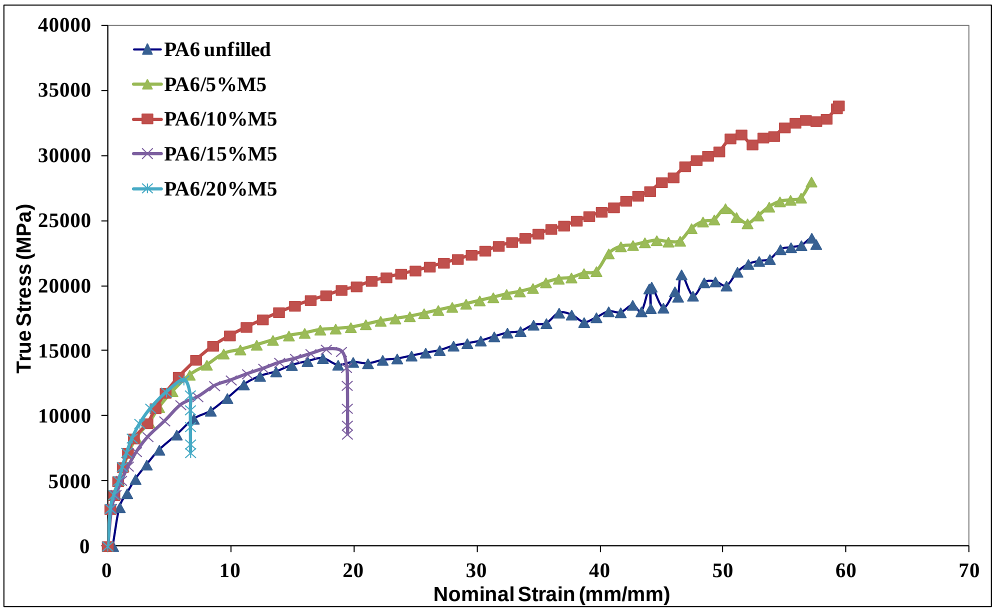

Fig.3: True stress-nominal strain behaviour for unfilled PA6 and PA6/M5 composites during uniaxial stretching.

Raman spectroscopy was carried out on PA6 and PA6/GNPs composites samples in order to explore the interaction between the nanoparticles and the polymer matrix. The two main bands in the spectrum for pure xGnPs are the G-band at ~1582 cm^{-1} and the 2D band at ~2685 cm^{-1} [21], which are clear in the spectra of the PA6/GNPs composites (Fig. 4). As expected the xGnPs bands get more pronounced when increasing the percentage of addition of nanoplatelets as the crystallinity increases [22-24]. There are also changes in the shape of the G and 2D bands of the nanocomposites, which are associated with the graphene layer thickness, dispersion, and polymer-GNP interphase [25, 26]. It can be noticed that the 2D peak broadens from 10% to 20%GNPs, which according to the literature is indicative of exfoliation of graphene layers [25].There is also a large increase in the size of the D band (around 1370 cm-1) for the composites, compared with the xGnPs which is associated with defects, mostly at the edges of graphene platelets [26, 27, 28].

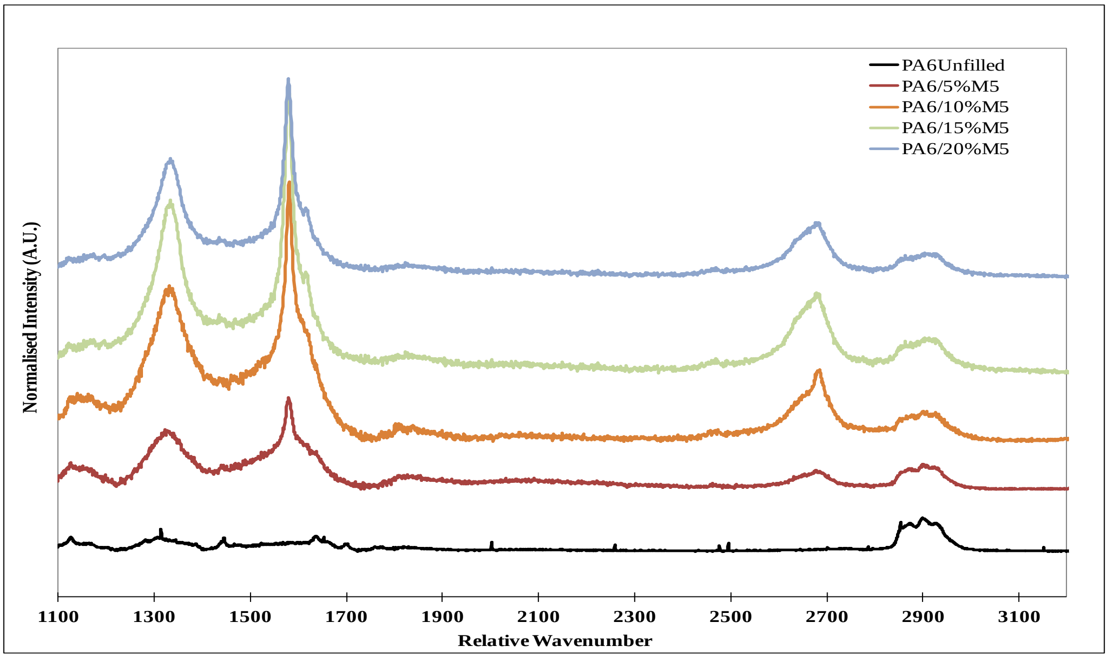

Fig. 4: Raman spectra for unfilled PA6 and PA6/M-5 xGnP composites.

Raman Spectroscopy was carried out on uniaxially stretched samples of PA6 and PA6/GNPs composites samples. By way of example, Raman spectra of PA6/15%M-5 composites that were unstretched and uniaxially stretched to a nominal strain of 20% are shown in Fig. 5. The shapes of the G and 2D bands become more pronounced and narrower for the uniaxially stretched sample due to the increase in crystallinity [29]. Some other researchers have investigated the interfacial interaction between the matrix and nanofillers during stretching using Raman spectroscopy [23, 29, 30]. Mai et al. reported the shifting of the G band peak (associated with tangential C-C bond stretching motions) to higher frequencies continuously with increasing draw ratio. This can be explained by the formation of a strong interaction between PA66 and MWCNTs and the disentanglements of MWCNTs improving dispersion into the polymer matrix [30]. In our studies was not possible to appreciate the up-shifting of the G-band, this may be due to the different type of stretching technique carried out and the effect in the interaction between GNPs and polymer matrix.

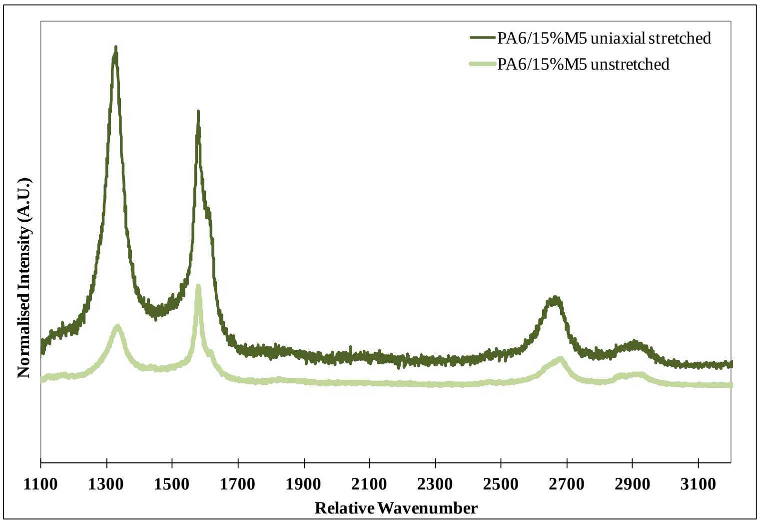

Fig. 5: Raman spectra for unstretched and uniaxial stretched PA6/15% M-5 composites.

From the melting endotherms shown in Fig.6, there is a broad melting peak in the unfilled PA6 and in the PA6/GNP composite materials starting around 210°C and peaking at ~223°C. The melting peak for γ-form crystals is approximately 213°C and for α-form crystals is approximately 221°C [31], clearly indicating the presence of α-form crystals but less-so for the γ-form crystals. From the WAXRD results in Fig. 2 there is no clear evidence of the γ-form crystals peak at 2θ = 21.4, and so the first DSC peak before the 221°C may be due to early melting of less perfect α crystallites. Thermal analysis using DSC was performed on the stretched samples to study the effect of stretching on the melting and crystallisation behaviour of PA6. Fig.6 shows the DSC thermograms for the first heating cycle for neat PA6 and the PA6/GNPs composites unstretched (Fig.6a) and uniaxial stretched (Fig.6b). The melting temperature (T_m) and crystalline content (X_c) were determined and are shown in Table 5. DSC thermograms in Fig. 6 and table 5 show a slight increase of the T_m and a more noticeable increase of the $\%X_c$ when the materials are uniaxially drawn. The maximum increase of $\%X_c$ is shown when the PA6/5%M-5 samples are uniaxial stretched with a 24% increase with respect to stretched, unfilled PA6 which is a 63% increase with respect to unstretched, unfilled PA6. It is also possible to see a change in shape (broadening) of the melting endotherms with increasing GNPs addition, suggesting a change in crystal type and perfection. This confirms that the overall increase in crystalline content is derived from a combination of heterogeneous nucleation induced by addition of GNPs to the PA6 matrix and strain induced crystallization [20].

DSC and Raman studies on the drawn samples show an increase in crystallinity as the GNP content increases due to the strain induced crystallization and possibly a γ-β transition during stretching occurred but cannot be confirmed by X-Ray analysis because the stretched sample size is too small for X-Ray characterization..

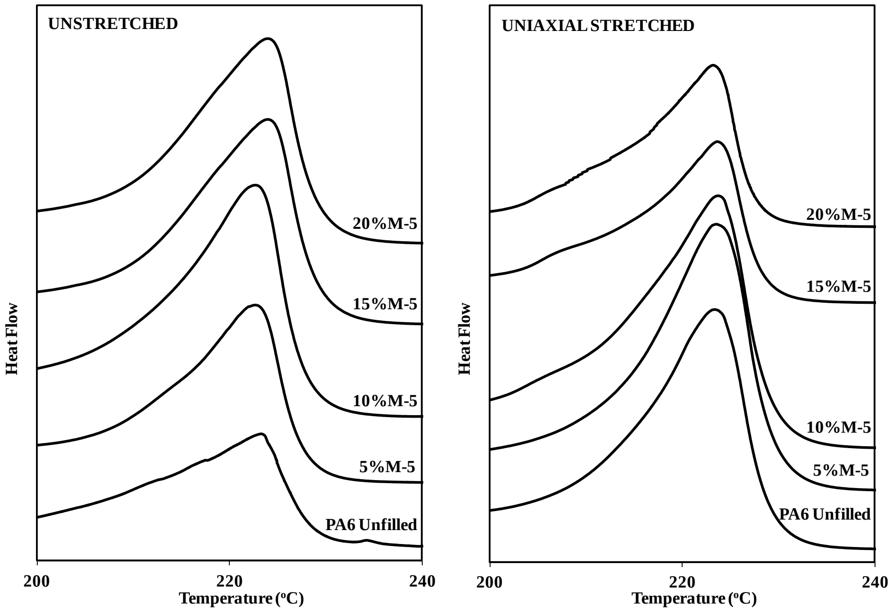

Fig.6: DSC thermograms showing melting endotherms (1st heating cycle) for unfilled PA6 and PA6/M-5 composites, (a) unstretched and (b) uniaxial stretched.

	UNSTRETCHED			UNIAXIAL STRETCHED			
	Tm (^{0}C)	Xc (%)	Impr* (%)	Tm (^{0}C)	Xc (%)	Impr** (%)	Impr* (%)
PA6 Unfilled	222.6	37.4		223.4	61.2		
PA6/ 5wt% M-5	222.6	70.4	88.1	223.6	76.1	24.3	63.5
PA6/ 10wt% M-5	222.6	78.2	109.0	223.7	86.0	40.6	103.3
PA6/ 15wt% M-5	224.0	81.9	118.7	224.2	92.5	51.2	129.9
PA6/ 20wt% M-5	224.7	83.2	122.2	224.9	94.9	55.1	147.1

*with respect to PA6 unfilled unstretched **with respect to PA6 unfilled uniaxial stretched

Table 5: Effect of M-5 GNPs addition on the thermal properties of unfilled PA6 and PA6/GNPs composites unstretched and uniaxially stretched.

Table 6 shows the change in electrical properties of the composites as the loading of particles is increased. The conductivity in the M-5 composites increases slowly with increasing loading and then increases at a faster rate after an electrical percolation threshold between 10-15 wt% GNPs, similar to observations of Young’s modulus. Fukushima et al. studied the electrical behaviour of PA6/xGnPs composites produced by melt-mixing and reported percolation thresholds at 7% vol for xGnP-15 and 10%vol for xGnP-1, but the xGnPs were treated prior to being incorporated into the matrix [32, 33].

Electrical conductivity analysis on uniaxial stretched samples was carried out. The uniaxial stretching slightly decreases the electrical conductivity (increasing the electrical resistivity) in PA6/M5 composites, as shown in table 6. Application of uniaxial stretching results in an increase in the distance between GNPs such that the electrically conducting GNPs network is interrupted. Previous studies have also reported an increase in resistivity for polymer/MWCNT composites [14, 20]. When the samples were annealed at 200°C (below the T_m of PA6), the volume resistivity of the uniaxial deformed sample decreased (conductivity increased), returning to a similar value obtained prior to stretching (See table 6). Annealing after uniaxial deformation permits some polymer chain relaxation and as a consequence increased GNP-GNP contacts to a similar level obtained prior to deformation recovering the electrical network [20, 34, 35].

		UNSTRETCHED	UNIAX STRET	ANNEALED
	GNP content ɸ [wt.%]	Vol. Resistivity (Ω.cm)	Vol. Resistivity (Ω.cm)	Vol. Resistivity (Ω.cm)
PA6 Unfilled	0	8.77E+14	9.37E+14	8.59E+14
PA6/ 5wt% M-5	5	1.53E+12	3.20E+12	2.75E+12
PA6/ 10wt% M-5	10	1.49E+10	3.51E+10	2.46E+10
PA6/ 15wt% M-5	15	9.49E+07	4.56E+08	1.12E+08
PA6/ 20wt% M-5	20	2.43E+06	2.59E+07	6.83E+06

Table 6: Volume resistivity of PA6 unfilled and PA6/M5 composites, unstretched, uniaxial stretched and annealed after stretching.

4 CONCLUSIONS

The addition of GNPs to PA6 matrix has the effect of dramatically increasing the crystallinity by 110-120% for 20%GNPs addition to the PA6 matrix due to the GNPs nucleation effect. A maximum increase of 378% in tensile modulus was achieved at a loading of 20wt% GNPs in PA6/M-5 composites, which can be attributed to the reinforcing effect of GNPs and their uniform dispersion in the PA6 matrix. The electrical conductivity increased as % GNPs increased, showing an increase of about 6 orders of magnitude on the addition of up to 15 wt% GNPs. Rheological and electrical percolation threshold for PA6/M-5 composites melt-mixed at 200rpm were both reached between 10-15 wt% GNPs.

Uniaxial stretching shows an increase in yield stress as the GNP content increases. The crystallinity increased when the samples were uniaxially drawn due to the strain induced crystallization with a 63% increase for PA6/5%M-5 uniaxial stretched samples with respect to PA6 unstretched. The uniaxial stretching slightly reduced the electrical conductivity in PA6/M-5 composites; however, the electrical network prior stretching was recovered when the samples were annealed due to polymer chain relaxation.

ACKNOWLEDGEMENTS

This article was made possible by NPRP grant # (NPRP5-039-2-014) from the Qatar National Research Fund (a member of Qatar Foundation). The statements made herein are solely the responsibility of the authors. The authors would like to thank Dr. Bronagh Millar for her expert contribution in the uniaxial stretching and characterization of composites.

REFERENCES

[1] J. R. Potts, D.R. Dreyer, C. W. Bielawski and R. S Ruoff, Graphene-Based Polymer Nanocomposites *Polymer*, **52** (1), 5-25, 2011.

[2] H. J. Salavagione, G. Martínez, and G. Ellis, Graphene-based polymer nanocomposites. Physics and Applications of Graphene—Experiments, *In-Tech*, Rijeka, 69, 2011.

[3] B. Li and W.H. Zhong, Review on polymer/graphite nano platelet nano composites, *Journal of Material Science*, **46**, 5595-5614, 2011.

[4] H. Kim, A.A. Abdala and C. Macosko, Graphene/polymer nanocomposites, *Macromolecules* **43** (16), 6515-6530, 2010.

[5] http://nobelprize.org/nobel_prizes/physics/laureates/2010/press.html

[6] http://www.rsc.org/chemistryworld/News/2010/June/14061001.asp.

[7] X.Y. Ji, Y.P. Cao and X.Q. Feng, *Modelling and Simulation in Materials Science and Engineering*, **18**, (4), 045005, 2010.

[8] L. T. Drzal and H. Fukushima, Expanded graphite, preparation of platelets, and nanocomposite products, Pat. Appl. Publ., U.S., 2004.

[9] L. T. Drzal and H. Fukushima, Expanded graphite and products produced therefore, Pat. Appl. Publ., U.S., 2006.

[10] K. Kalaitzidou and H. Fukushima and L.T. Drzal, Multifunctional Polypropylene Composites Produced by Incorporation of Exfoliated Graphite Nanoplatelets, *Carbon*, **45**, 1446-1452, 2007.

[11] B. Mayoral, T. McNally and G. Garrett, Effect of screw configuration profiles on the dispersion of MWCNTs in a Poly (propylene) Matrix, *Macromolecular Mat. Eng.*, **299**, 748-756, 2014.

[12] J.A. King, M.D. Via, J.M. Keith and F.A. Morrison, Effects of Carbon Fillers on Rheology of Polypropylene-based Resins, *Journal of Composites Materials,* **43**, 25, 3073-3089, 2009.

[13] P. Pötschke, M. Abdel-Goad, I. Alig, S. Dudkin and D. Lellinger, Rheological and dielectric characterization of melt mixed-MWCNTs composites, *Polymer,* **49**, 974-984, 2004.

[14] F. Du, R.C. Scogna, W. Zhou, S. Brand, J.E. Fischer and K. Winey, Nanotube networks in polym nanocomps: Rheology and electrical conductivity, *Macromol.*, **37**, 24, 9048-9055, 2004.

[15] M. R. Nobile, *Rheology of polymer-carbon nanotube composite melts, Polymer*-carbon nanotube composites: Preparation, properties and applications, McNally, T., Pötschke, P., Eds., Vol. **15**, 428-481, Woodhead Publishing, Cambridge, 2011.

[16] B. Mayoral, J. Lopes and T. McNally, Influence of Processing Parameters During Small-Scale Batch Melt Mixing on the Dispersion of PP/MWCNTs, *Macrom. Mat. Eng,* **298**, 1-13, 2013.

[17] T.D. Thanh, L. Kapralkova, J. Hromadkova and I. Kelnar, *Eur. Polym. J*., **50**, 39, 2014.

[18] J. A. King, M. D. Via, F. A. Morrison, K. R. Wiese, E. A. Beach, M. J. Cieslinski and G. R. Bogucki, *Journal of Composites Materials*, **46**(9), 1029, 2012.

[19] W. Liu, I. Do, H. Fukushima and L.T. Drzal, Influence of Processing on Morphology, Elect. Cond. and Flexural Props of xGNPs–PA Nanocomposites, *C. Letters*, **11**, 4, 279-284, 2010.

[20] B. Mayoral, P. R. Hornsby, T. McNally, T. Schiller, K. Jack and D. J. Martin, Quasi-Solid State Uniaxial and Biaxial Deformation of PET/MWCNT Composites, *RSC Adv.*, **3**, 5162-5183, 2013.

[21] XG Science xGNP-M grade Technical Data Sheet http://xgsciences.com/xGnP-M DataSheet.pdf

[22] S. R. Ahmad, R. J. Young and I. A. Kinloch, Raman Spectra and Mechanical Properties of Graphene/PP Nanocomposites, *Int. J. Chemical Engineering and Applications*, **6**, 1, 2015.

[23] A. Crawford, E. Silva, K. York and C. Li, Raman Spectroscopy: A Comprehensive Review *Department of Textile Engineering, Chemistry and Science North Carolina State University*.

[24] Li, L.; Li, C. Y.; Ni, C.; Rong, L.; Hsiao, B. Structure and Crystallization Behaviour of Nylon 66 /MWCNTs nanocomposites at low carbon nanotube contents, *Polymer*, **48**, 3452-3460, 2007.

[25] A. C. Ferrari, J. C. Meyer, V. Scardaci, C. Casiraghi, M. Lazzeri, F. Mauri, S. Piscanec, D.Jiang, K. S. Novoselov, S. Roth and A. K. Geim, Raman Spectrum of Graphene and Graphene Layers, *Physical Review Letters* **97,** 187401-4, 2006.

[26] A. Jorio, E. H. Martins Ferreira, L. G. Cançado, C. A. Achete and R. B. Capaz, Measuring Disorder in Graphene with Raman Spectroscopy, *Physics and Applications of Graphene - Experiments, Ed.* Dr. Sergey Mikhailov, InTech, 2001.

[27] Thermo Fisher Scientific Inc. Application Note, 51946, 2010.

[28] C. Casiraghi, A. Hartschuh, H. Qian, S. Piscanec, C. Georgi, A. Fasoli, K. S. Novoselov, D. M. Basko, A. C. Ferrari, Raman Spectroscopy of Graphene Edges, *Nanolett*, **9**, 4, 1433-1441, 2009.

[29] L. Gong, R. J. Young, I. A. Kinloch, I. Riaz, R. Jalil, and K. S. Novoselov, Optimizing the reinforcement of polymer-nanocomposites by Graphene, *ACSnano* , **6**, (3), 2086–2095, 2012.

[30] F. Mai, D. Pan, X. Gao, M. Yao, H. Deng, K. Wang, F. Chen and Q. Fu, Extension-Induced Mech Reinf. Melt-Spun Fibers of PA66/MWCNT Composites. *Polym. Int.*, **60**,1646-1654, 2011.

[31] M. N. Bureau, J. Denault, K.C. Cole and G. D. Enright, The role of crystallinity and reinforcement in the mechanical behaviour of PA6/clay, Society of Plastics Engineers, 2002.

[32] H. Fukushima, L.T. Drzal, B.P. Rook and M.J. Rich, Thermal Conductivity of Exfoliated Graphite Nanocomposites, *J.Thermal Anal Calor*, **85** (1), 235-238, 2006.

[33] H. Fukushima and L.T. Drzal, Nylon - xGnP nanocomposites with enhanced mechanical, electrical and thermal properties, *NSTI Nanotech Technical Proceedings*, **1**, 282-285, 2006.

[34] I. Alig, D. Lellinger, S. Dudkin and P. Pötschke, Conductivity spectroscopy on melt processed PP/MWCNT composites: recovery after shear and crystallization, *Polymer,* **48**, 1020-1029, 2007.

[35] I. Alig, T. Skipa, D. Lellinger and P. Pötschke, Destruction and formation of a conductive CNTs network in polymer melts: rheology and conductivity, *Polymer,* **49**, 3524-3532,2008.